RSC Advances

ROYAL SOCIETY OF CHEMISTRY

www.rsc.org/advances

Figure 6

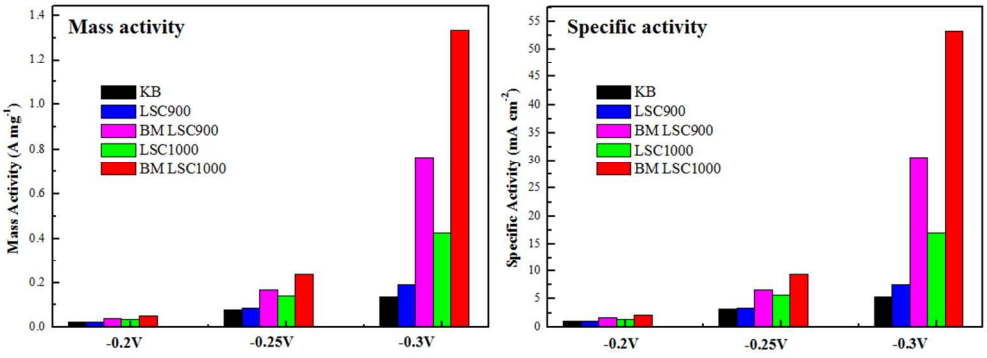

The perovskite LSC exhibited better catalytic performance than conventionally used KB and improved the reversibility of the O2 electrode
306x120mm (96 x 96 DPI)

Cite this: DOI: 10.1039/c0xx00000x

www.rsc.org/xxxxxx

ARTICLE TYPE

The bifunctional electrocatalytic activity of perovskite $La_{0.6}Sr_{0.4}CoO_{3-\delta}$ for oxygen reduction and evolution reactions

Mi Young Oh[a], Jeong Sook Jeon[b], Jong Ju Lee[b], Pil Kim[a, b, c], Kee Suk Nahm[a, b, c, *]

Received (in XXX, XXX) Xth XXXXXXXXX 20XX, Accepted Xth XXXXXXXXX 20XX

DOI: 10.1039/b000000x

Perovskite $La_{0.6}Sr_{0.4}CoO_{3-\delta}$ was synthesized by the Pechini method at different synthetic conditions and examined as a bi-functional catalyst for oxygen reduction reaction (ORR) and oxygen evolution reaction (OER). As the calcination temperature increases, the particle size and purity of the $La_{0.6}Sr_{0.4}CoO_{3-\delta}$ increases, indicating the formation of highly pure $La_{0.6}Sr_{0.4}CoO_{3-\delta}$ at higher calcination temperatures. The specific surface area of the perovskite oxides is increased by ball milling, which shows the improvement of the electrocatalytic activity. The electrocatalytic activities of all the prepared $La_{0.6}Sr_{0.4}CoO_{3-\delta}$ are much better than that of Ketjen black. The catalytic activity of the $La_{0.6}Sr_{0.4}CoO_{3-\delta}$ for both ORR and OER was systematically studied by combining their structural and electrochemical properties. The $La_{0.6}Sr_{0.4}CoO_{3-\delta}$ was then employed as an air cathode catalyst in lithium-air battery to investigate the battery performance.

1. Introduction

Lithium–air battery has a theoretical energy density 10 times higher than that of lithium–ion battery. In addition, it has the advantages of light weight and low cost because oxygen in air is used as active material in air electrode. This has drawn a great research interest in lithium–air battery technology to be applied in large energy storage devices [1–5].

In order to commercialize the lithium–air battery, however, there are many problems to be technically solved [6, 7]. Particularly, since lithium peroxide (Li_2O_2) produced at the cathode during discharge process is in solid phase, it could blocks the pores on the porous carbon electrode surface and reduce the contact area of oxygen and electrolyte, resulting in the degradation of lithium–air battery performance [8, 9]. Since the Li_2O_2 acts as an insulator, moreover, the electron transfer is also not easy and high overpotential will be required to decompose Li_2O_2 and Li_2O into O_2 and Li on recharging. This high overpotential causes some side reactions which accelerate electrolyte decomposition and carbon electrode corrosion. It has been also reported that irreversible discharge products such as Li_2CO_3 and $LiRCO_3$ causes the degradation in the cycle life of lithium–air battery [10–14].

There have been wide and intensive researches to overcome these problems, and to develop new promising catalysts with high reactivity at the air electrode [15, 16]. So far various metals and metal oxides including Pt have been widely employed as air cathode catalyst in fuel cells and metal air batteries [15, 17–32]. Recently, perovskite oxides have been investigated as active catalyst at air cathodes in lithium-air batteries. The catalytic performance of perovskite oxides like $CaMnO_3$ [24], $La_{0.8}Sr_{0.2}BO_3$ (B=Co, Mn, Fe) [25–27], La_2NiO_4 [28], $La_{0.6}Ca_{0.4}Co_{0.8}Fe_{0.2}O_3$, $La_{0.6}Sr_{0.4}Co_{0.2}Fe_{0.8}O_3$, $La_{0.8}Sr_{0.2}Fe_{0.8}Mn_{0.2}O_3$ [29], $Ba_{0.9}Co_{0.5}Fe_{0.4}Nb_{0.1}O_3$ [30], $LaFeO_3$ [31] and $LaNi_{1-x}Mg_xO_3$ [32], and their A- and B- site substituted oxides have been examined. Most of the reported works have been focused on the charge/discharge and cycle performance of the lithium-air battery. But a detailed and systematic study for electrochemical properties of the materials has not yet been fully made to explain the electrocatalytic properties. Among the reported perovskite catalysts, furthermore, $La_{0.6}Sr_{0.4}CoO_{3-\delta}$ has been investigated as a promising electrode material in fuel cells [33–36], because the $La_{0.6}Sr_{0.4}CoO_{3-\delta}$ composition shows higher oxide ion conductivity and electronic conductivity compared to the other perovskite oxides [37–39]. The $La_{0.6}Sr_{0.4}CoO_{3-\delta}$ composition has been mainly studied for electrochemical characteristics for the application as cathode electrode in solid state fuel cells to reduce the electrode resistance. As far as we have investigated, however, there are no reports on the application of $La_{0.6}Sr_{0.4}CoO_{3-\delta}$ as air cathode catalyst for lithium-air batteries though other compositions of LSC have been reported. Zhao et al.[27] synthesized hierarchical mesoporous perovskite $La_{0.5}Sr_{0.5}CoO_{2.91}$ nanostructures for the application of Li-air batteries. They observed that the $La_{0.5}Sr_{0.5}CoO_{2.91}$ composition produced better electrochemical properties and cell performances, which exhibited ultrahigh discharge capacities over 11,000 $mAh \cdot g^{-1}$.

In this work, we synthesized perovskite $La_{0.6}Sr_{0.4}CoO_{3-\delta}$ (LSC) which possesses relatively high electron conductivity and ionic conductivity using the Pechini method. To decide an optimum synthetic condition, the perovskite $La_{0.6}Sr_{0.4}CoO_{3-\delta}$ (LSC) was synthesized at different drying and calcination temperatures. The ball milling technique was utilized to increase the specific surface area of the oxides. Various physicochemical characterization

techniques have been utilized to investigate the crystalline structure and morphology of the synthesized perovskite oxides. The electrocatalytic properties of thus prepared perovskite $La_{0.6}Sr_{0.4}CoO_{3-\delta}$ oxides were first examined in O_2 saturated KOH aqueous solution using various electro–analytic techniques such as cyclic voltammetry (CV) and linear sweep voltammetry (LSV). The CV, ORR and OER studies were also carried out for Ketjen black (KB) and Pt/C for comparative analysis with that of our prepared $La_{0.6}Sr_{0.4}CoO_{3-\delta}$ oxides. The synthesized LSC was employed as electrocatalyst in the air cathode of lithium–air battery and the charge/discharge cyclability was analyzed for the test cells. On the basis of the experimental analysis, the catalytic activities of the synthesized $La_{0.6}Sr_{0.4}CoO_{3-\delta}$ for ORR and OER were systematically studied with respect to their structural properties.

The main text of the article should appear here. Headings and subheadings should be formatted using the relevant button from the "Apply Style" dialog box (see the RSC Tools toolbar above).

A tab stop has been set in the style to allow for easy indenting of text (although the first paragraph and paragraphs that follow headings should not be indented).

2. Experimental

2.1. Synthesis of perovskite $La_{0.6}Sr_{0.4}CoO_{3-\delta}$

$La_{0.6}Sr_{0.4}CoO_{3-\delta}$ has been synthesized by Pechini method which is well known for the synthesis of perovskite oxides [40-41]. The optimum synthetic condition was investigated by varying the synthetic conditions. All the chemical precursors ($La(NO_3)_3$▪$6H_2O$ (99.9%, Sigma-Aldrich), $Sr(NO_3)_2$ (99%, Sigma-Aldrich), and $Co(NO_3)_2$▪$6H_2O$ (97.7%, Sigma-Aldrich)) were chemical grade and used as received without any further purification. A stoichiometric molar ratio of 0.6:0.4:1.0 of $La(NO_3)_3$, $Sr(NO_3)_2$, and $Co(NO_3)_2$ was dissolved in DI water to prepare 0.03M of a mixed solution. Citric acid (99.5%, Sigma-Aldrich) was added in the mixed solution to form a metal complex compound. Later ethylene glycol (99%, Sigma-Aldrich) was added in the mixed solution and stirred at 80°C for 2 hours. While stirring, the gel is formed which indicates the formation of poly resin and the gel was dried at constant temperatures of 80°C and 200°C. Thus formed polymer resin was carbonized at 400°C for 1 hour to remove residues such as nitric acid and organic chemicals. Then the resin was grinded in a crucible to form powders. Then the prepared powders were calcined for 4 hours at temperature range of 800 ~ 1100°C. Thus prepared LSC were further pulverized with a ball miller to investigate size effect of the LSC. Throughout this paper, LSC800, LSC900, LSC1000 and LSC1100 represent the $La_{0.6}Sr_{0.4}CoO_{3-\delta}$ synthesized at the calcination temperatures of 800, 900, 1000, and 1100°C, respectively, while BM LSC900 and BM LSC1000 depict ball milled LSC900 and LSC1000, respectively.

2.2 Characterizations of $La_{0.6}Sr_{0.4}CoO_{3-\delta}$

Structural analysis of the synthesized $La_{0.6}Sr_{0.4}CoO_{3-\delta}$ was carried out with X-ray diffractometer (XRD) using a CuKα (λ=1.54059 Å) target in the 2θ range of 10~100°. In order to examine particle size, distribution, and morphology, field emission scanning electron microscopy (FESEM) and transmission electron microscopy (TEM) were performed. In addition, Brunauer-Emmett-Teller (BET) technique was used to characterize specific surface area, pore size, and pore volume of the LSC.

Electrocatalytic measurements for oxygen reduction reaction (ORR) and oxygen evolution reaction (OER) were carried out on a computerized potentiostat instrument (model CHI700C) at room temperature in a three electrode system using 0.1M KOH as electrolyte. For cyclic voltammetry (CV) measurement, a glassy carbon disk electrode was employed as the working electrode. The linear sweep voltammetry (LSV) was recorded with a rotating ring glassy carbon disk electrode (RRDE, 5.61mm in diameter) as the working electrode, at a scan rate of 5mV s^{-1}, with a disk rotation rate of 1600 rpm.

2.3. Preparation of electrodes

The synthesized LSC was used as air cathode catalyst, and KB (Ketjen Black, EC600JD) and 30wt% Pt/C (Premetek Co.) were also employed for comparison. For CV, ORR and OER studies, the synthesized LSC was mixed with carbon powder (Cabot Vulcan XC-72) in the weight ratio of 3:7 to ensure sufficient electronic conductivity. 10mg of as-prepared catalyst was dispersed ultrasonically in 150μL of diluted nafion alcohol solution (5 wt%) dissolved in isopropyl alcohol (IPA), and about 13.5μL of the suspension was pipetted onto a glassy carbon substrate. Pt wire and Hg/HgO were used as the counter and the reference electrodes, respectively. Prior to measurement, O_2 was bubbled directly into the cell for at least one hour.

For lithium-air battery studies, the air cathodes were prepared by mixing as–prepared LSC catalyst and KB conductive carbon in the ratio of 1:2 with teflonised acetylene black (TAB) binder (60%) in isopropyl alchohol (IPA). The mixture was prepared into a fine pellet of about 1cm diameter and the pellet was pressed on a Ni mesh current collector with a diameter of 1.2cm. Thus prepared electrode is then dried in vacuum at 100°C for 12 hours and used as air cathode in Li air battery. Lithium metal foil was used as anode and electrolyte used was prepared by dissolving 1M LiTFSI in TEGDME. A Swagelok test cell was used for the fabrication of lithium-air battery and the cell test was carried out under oxygen flow (10cc min^{-1}) at a current density of 0.1mA cm^{-2} in a cut-off voltage range of 2.0–4.3V.

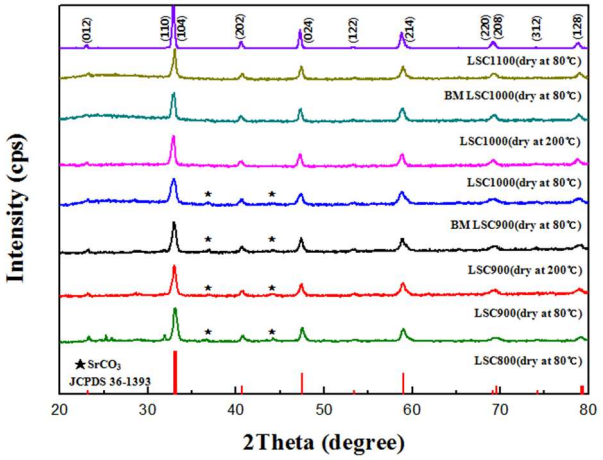

Fig.1 X-ray diffraction patterns of $La_{0.6}Sr_{0.4}CoO_{3-\delta}$ synthesized at different drying and calcination temperatures

Cite this: DOI: 10.1039/c0xx00000x

www.rsc.org/xxxxxx

ARTICLE TYPE

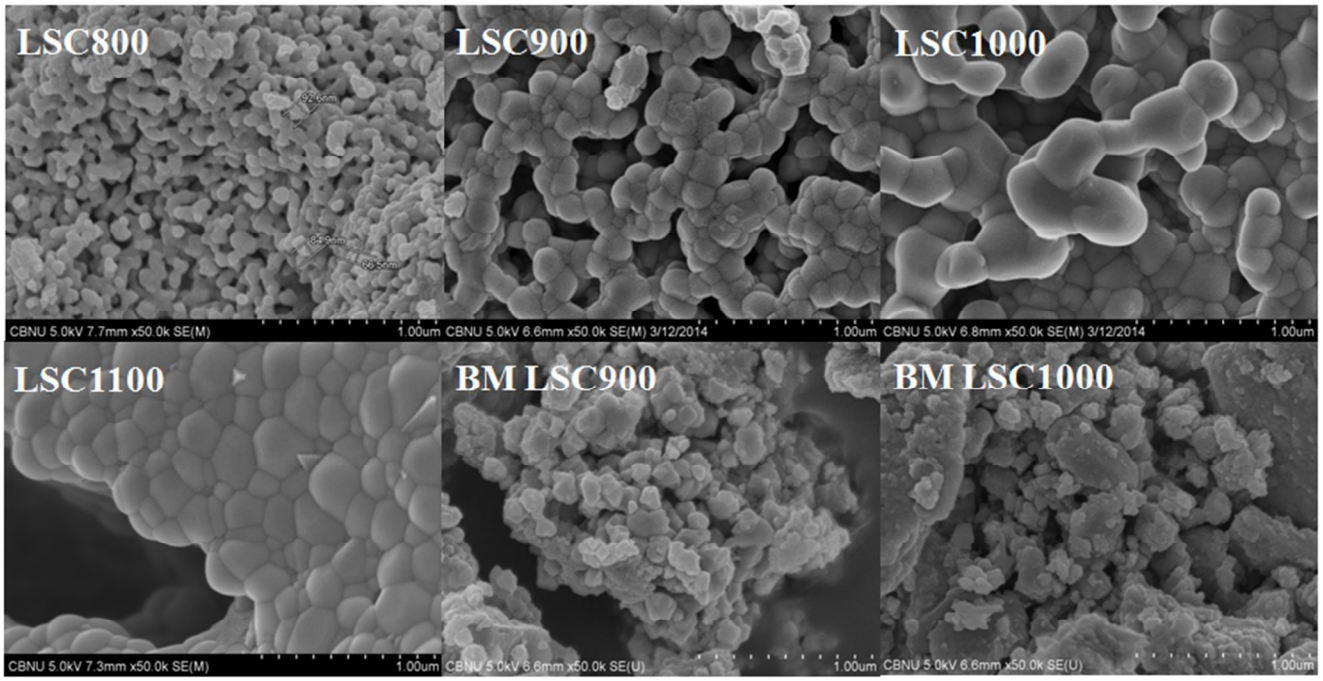

Fig.2 FESEM images of LSC and ball milled LSC

3. Results and Discussion

3.1 Structural properties of perovskite $La_{0.6}Sr_{0.4}CoO_{3-\delta}$

Figure 1 shows XRD spectra of the perovskite $La_{0.6}Sr_{0.4}CoO_{3-\delta}$ synthesized as a function of drying and calcination temperatures. All the synthesized LSC materials exhibit one main characteristic peak at $2\theta = 33^{o}$ which corresponds to the (110)/ (104) plane of LSC. All the peaks observed from the spectra well coincides with the previously reported XRD spectrum of $La_{0.6}Sr_{0.4}CoO_{3-\delta}$ [42], indicating the successful synthesis of LSC. For the case of LSC oxides which were synthesized at drying temperatures of 80°C and 200°C and calcination temperatures of 800 and 900°C, the $SrCO_3$ impurity phase is observed [38, 43-45]. But the $SrCO_3$ and other impurity peaks clearly disappear from the spectra of the LSC synthesized at 1000 and 1100°C. It is noteworthy that regardless of the drying temperatures when the samples were calcined at elevated temperatures up to 1000°C the impurities disappeared. Therefore, it can be confirmed that the purity of the perovskite LSC is mainly influenced by the calcination temperature rather than the drying temperature. Consequently the LSC oxides synthesized at higher calcination temperatures exhibit better crystallinity, while at lower calcination temperatures they exhibit poor crystal structure. This has been observed in previous reports on the synthesis of other perovskites [39, 42]. XRD measurements reveal that stable and pure perovskite $La_{0.6}Sr_{0.4}CoO_{3-\delta}$ structure is formed at up to 1000°C.

Primary particle size of the as-synthesized perovskite oxides LSC800, LSC900, LSC1000 and LSC1100 were calculated using the Scherrer equation from the XRD spectra at $2\theta = 33°$ which corresponds to the main characteristic peak [46, 47]. The primary particle sizes of LSC800, LSC900, LSC1000 and LSC1100 are found to be 15.7, 18.55, 19.54 and 22.2 nm, respectively. This explains that the primary particle size increases with the increase of calcination temperatures. In general, it has been reported that the particle size of chemically synthesized solid particles increases as the calcination temperature increases [39, 42]

Figure 2 shows the FESEM images of the synthesized LSCs. It is seen that the primary particles combine to make larger sized secondary particles. The secondary particle sizes are in the range of 60-100 nm, 150–200nm, and 200–450nm for LSC800, LSC900, and LSC1000, respectively. For the case of LSC1100, however, the primary particles aggregate to form a big sized secondary particle. This clearly manifests that the primary particles with nm sizes aggregate together to form larger sized secondary particles and the average size of the secondary particles increases with calcination temperatures. In order to confirm this behavior, the aggregated secondary particles of LSC1000 were investigated with TEM analysis. As shown in Fig.3, it is clearly manifested that the primary particles get

Cite this: DOI: 10.1039/c0xx00000x

www.rsc.org/xxxxxx

ARTICLE TYPE

Table 1 Specific surface area of $La_{0.6}Sr_{0.4}CoO3-\delta$; peak potential and peak current from cyclic voltammograms and, onset potential and limiting current from oxygen reduction reaction curves for $La_{0.6}Sr_{0.4}CoO_{3-\delta}$ perovskite catalysts

Sample	Specific Surface area ($m^2 g^{-1}$)	Peak Potential (V)	Peak Current (mA)	Onset Potential (V)	Limiting Current (mA)
LSC900	1.23	-0.22	0.147	-0.155	0.832
BM LSC900	3.21	-0.22	0.227	-0.149	0.962
LSC1000	0.20	-0.22	0.167	-0.143	0.962
BM LSC1000	2.11	-0.21	0.213	-0.141	0.920

together to form a secondary particle. Also, the high–resolution TEM image (inset of Fig. 3) shows that the lattice fringes of each particle is 0.28nm which corresponds to (110) plane of XRD.

In order to see the effect of the surface area on the electrocatalytic activity, the ball milling technique was utilized to increase the specific surface area of the LSC 900 and LSC 1000. The ball milling effect and electrochemical study were considered for the LSC oxides synthesized at 900 and 1000°C because the $SrCO_3$ impurity phase was observed at 900°C, while it disappeared at 1000°C. Fig. 2 shows the FESEM images of LSC900 and LSC1000 after ball milling at 200rpm for 5 hours. It can be seen that both the BM LSC900 and BM LSC1000 show the disintegration of the particles, but the degree of the pulverization is slightly different for the two perovskite oxides. The particles of BM LSC900 are uniformly distributed with the size of ~100nm, while BM LSC1000 is disintegrated into smaller particles with various sizes. This indicates that LSC1000 calcined at higher temperature is a little bit harder in structure than LSC900 calcined at comparatively lower temperature, though the crystalline quality of the perovskite oxides was not affected by ball milling (Fig. 1).

But peak current of LSC1000 is higher than that of LSC900. In order to explain why LSC1000 shows better reaction performance than LSC900, the specific surface areas of LSC1000 and LSC900 were measured using a BET technique. As listed in Table 1, LSC1000 has the smallest specific surface area of $0.2 m^2 g^{-1}$ which is lower than that of LSC900 with $1.23 m^2 g^{-1}$. This is because the particle size increases almost twice by agglomeration during calcination as the temperature increases. It is interesting to see that LSC1000 shows better reaction performance than LSC900 although LSC900 showed higher specific surface area than LSC 1000. It can be considered that the better reaction performance of LSC1000 is due to the better crystallinity and purity (without any impurities). It is believed that LSC900 exhibits inferior catalytic activity due to the $SrCO_3$ impurity as observed in XRD

3.2 Electrochemical properties of perovskite $La_{0.6}Sr_{0.4}CoO_{3-\delta}$

The electrocatalytic activities were studied for the perovskite $La_{0.6}Sr_{0.4}CoO_{3-\delta}$ oxides synthesized at 900 and 1000°C using various electro–analytic techniques such as cyclic voltammetry (CV) and linear sweep voltammetry (LSV) to compare the LSC samples with and without impurities. Figure 4 shows the cyclic voltammogram of the perovskite $La_{0.6}Sr_{0.4}CoO_{3-\delta}$ measured at a scan rate of 50mV s^{-1} in O_2 saturated 0.1M KOH solution. For both LSC900 and LSC1000, a peak is observed at almost same potential from cathodic reduction curves. The cyclic voltammogram of LSC1000 was also measured at N_2 atmosphere under the same experimental conditions. The CV curve of LSC 1000 under N_2 atmosphere exhibits the behavior of double layer capacitance without evolution of the peak. This identifies that the peak observed under O_2 atmosphere is due to the oxygen reduction reaction at the cathode. The values of peak potential and current were deduced from the CV curves in Fig. 4 and listed in Table 1. The peak potentials do not show any apparent difference for the LSC catalysts synthesized at different conditions. But peak current of LSC1000 is higher than that spectrums.

Peak currents of BM LSC1000 and BM LSC900 are higher than those of LSC1000 and LSC900. This confirms that among all the synthesized LSC, ball milled LSC shows the highest catalytic activity for ORR. We also measured the specific surface area of the ball milled LSC900 and LSC1000. After ball milling, it is seen that the specific surface areas of both LSC900 and LSC1000 increase due to the reduction of the particle size. The specific surface area of BM LSC 900 was 3.21 $m^2 g^{-1}$ while that of BMLSC 1000 2.11 $m^2 g^{-1}$. This is due to the reduction in particle size after ball milling as discussed above. The increase in catalytic activity of the ball milled LSC catalysts is due to the increase in specific surface area after the ball milling, which increases the gas-liquid-solid three phase interface necessary for

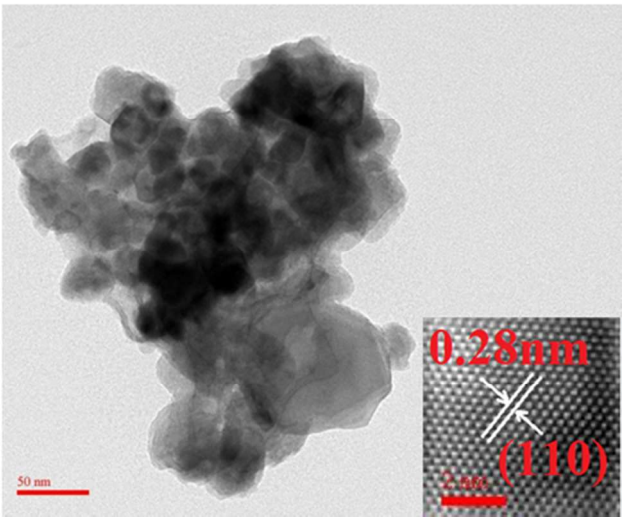

Fig.3 TEM image of LSC1000

electrochemical reaction. While comparing the catalytic activity of BM LSC900 and BM LSC1000 for ORR, however, BM LSC900 shows slightly higher peak potential than BM LSC1000. This might be due to the harder structure of BM LSC1000. As we could see from Fig. 4, the particles of BM LSC1000 were not uniformly disintegrated after the ball balling, showing slightly lower specific surface area as shown Table 1.

The catalytic activity of the synthesized $La_{0.6}Sr_{0.4}CoO3$-δ for ORR was also investigated by measuring linear sweeping voltammogram in O_2 saturated 0.1M KOH solution at a scan rate of 5mV s^{-1} over an electrode rotation rate of 1600rpm, as shown in the left side of Fig. 5. For comparison, ORR activity was also measured on KB and Pt/C under the same experimental conditions. The onset potential and limiting current of the LSC catalysts were inferior to that of Pt/C, but much better than KB. The onset potential data shows that LSC1000 has lower potential for ORR than LSC900 and the ball milling also decreases the potential of the perovskite catalyst. Meanwhile, the LSC1000 exhibits higher limiting current of 0.962mA in comparison with LSC900 (0.832mA) even though the former showed lower specific surface area than the latter. It is considered that the $SrCO_3$ impurity [48] present in LSC900 is again the reason for these obtained results. In this case, it is considered that the catalytic activity is more influenced by impurities than by specific surface area. After the ball milling, meanwhile, BM LSC900 shows lower onset potential and higher limiting current than LSC900. This increase in the catalytic activity of BM LSC900 can be attributed to the increase in specific surface area upon ball milling. In the case of LSC1000 the onset potential improves after the ball milling, but the limiting current slightly deteriorates. From our observations, it seems that the ball milling process is beneficial to increase the catalytic activity of the LSC. Generally upon ball milling reactive defects might be formed in large number which could be another reason for the increase in catalytic activity of LSC 900 upon ball milling. In catalytic reactions, specific surface area and chemical properties of catalysts employed are important parameters to decide the catalytic activity [38, 44, 48]. In general, the increase of the specific surface area results in the increase of the catalytic

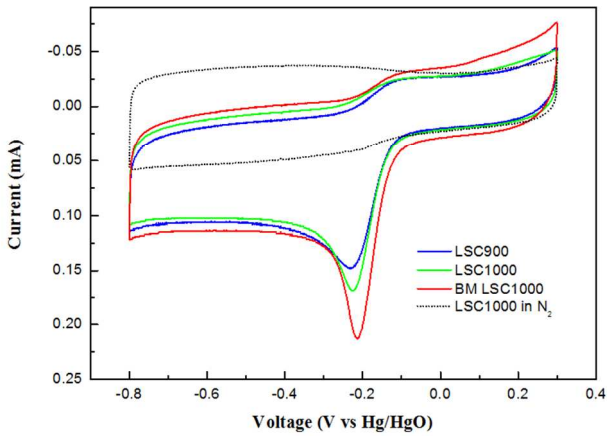

Fig.4 cyclic voltammogram of $La_{0.6}Sr_{0.4}CoO_{3-\delta}$ perovskite catalysts in O_2 saturated 0.1M KOH solution at 50mV s^{-1}

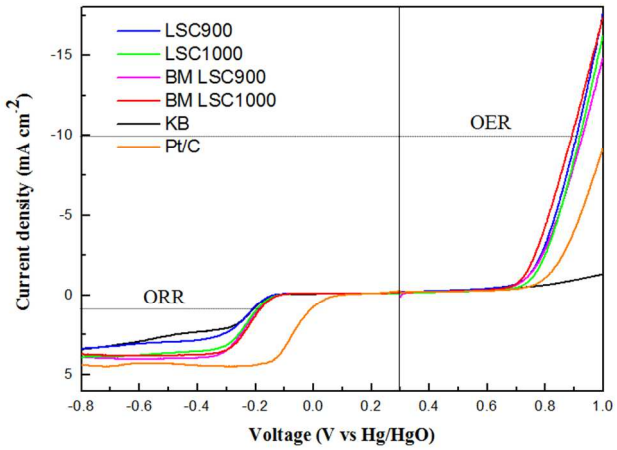

Fig.5 Oxygen electrode activities with the oxygen reduction and evolution reaction potential windows of the $La_{0.6}Sr_{0.4}CoO_{3-\delta}$ perovskite catalysts in oxygen-saturated 0.1M KOH solution at 1600 rpm with a scan rate of 5mV s^{-1}

performance, but the concentration of active sites on catalyst surface is more important in resulting in determining the catalytic performance. We believe some more fundamental study such as surface state research of the LSC is necessary in future to understand this process clearly.

We also investigated the catalytic activity of the synthesized perovskite catalysts for OER. The polarization curves were measured during the anodic potential scan up to 1.0V vs. Hg/HgO in 0.1M KOH solution at a scan rate of 5mV s^{-1} with rotation rate of 1600rpm as shown in the right side of Fig. 5. From the OER characteristics, all the synthesized perovskite catalysts exhibit much better catalytic activity for OER than Pt/C and KB. The overall electrochemical reaction of lithium–air battery can be expressed as $2(Li^+ + e^-) + O_2 \rightleftarrows Li_2O_2$; during which oxygen reduction reaction (ORR) takes place on discharge process (forward), followed by the oxygen evolution reaction (OER) on charging (reverse). Generally the decomposition of solid–state discharge products, Li_2O_2, on charging requires very large potentials, which lower a round trip efficiency of the battery [10]. Hence it is essential to develop an efficient ORR and OER bifunctional electrocatalyst to reduce the overpotential in the lithium–air batteries. All the $La_{0.6}Sr_{0.4}CoO_{3-\delta}$ synthesized in this

Cite this: DOI: 10.1039/c0xx00000x

www.rsc.org/xxxxxx

ARTICLE TYPE

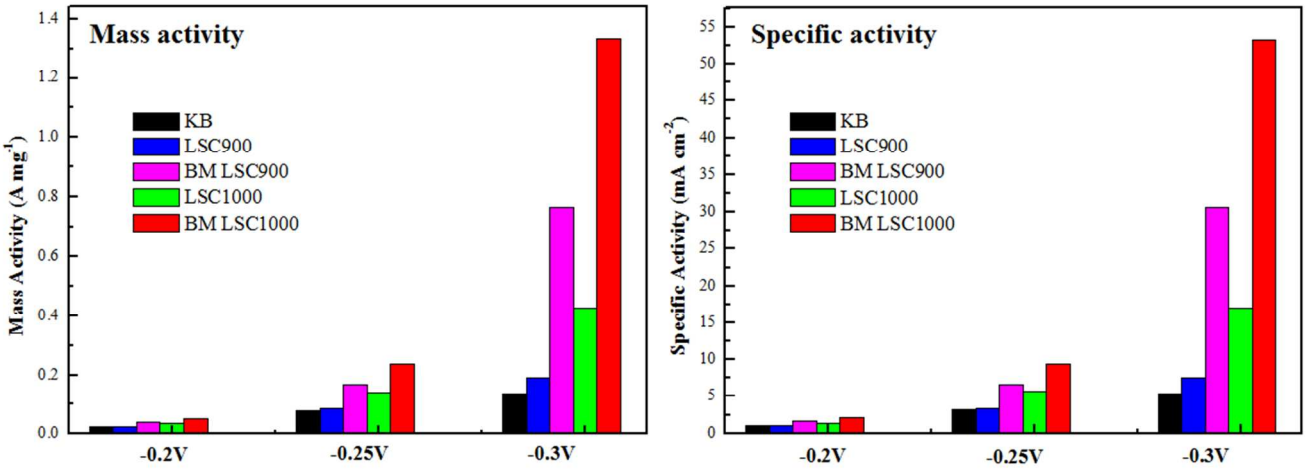

Fig.6 Mass and specific activities of the $La_{0.6}Sr_{0.4}CoO_{3-\delta}$ perovskite catalysts obtained at -0.2, -0.25 and -0.3V (vs. Hg/HgO; 0.1M KOH) from ORR data

experiment shows better catalytic activity for ORR than KB; they also exhibit superior catalytic activity for OER than Pt/C and KB. This indicates that the perovskite catalysts can be effectively employed as a cathode catalyst in lithium–air batteries.

To assess the overall oxygen electrode activity, the potential difference between the ORR and the OER curves was calculated and the detail is given in Table 2. The potential at which the current reaches its half maximum value was selected for the ORR. Therefore an ORR current of 1mA cm^{-2} was selected which approximates the half–wave potential. Activities for the OER were judged by the potential required to oxidize water at 10mA cm^{-2}, a convention commonly used in the OER literature [49, 50]. In this work, therefore, the potentials of the OER were measured at 10mA cm^{-2}, which corresponds to the current density of water oxidation. Among all the synthesized perovskite oxides, it can be seen from the Table 2 that the BM LSC1000 has the least value with oxygen electrode activity of 1.08V. This confirms that the perovskite oxides show superior catalytic activities for both ORR and OER.

Table 2 Comparison of overall catalytic activities of $La_{0.6}Sr_{0.4}CoO_{3-\delta}$ perovskite catalysts

Sample	ORR: E(V) at I = 1 $mAcm^{-2}$	OER: E(V) at I = 10 $mAcm^{-2}$	Oxygen electrode Δ (OER-ORR):E(V)
LSC900	-0.211	0.909	1.120
BM LSC900	-0.196	0.921	1.117
LSC1000	-0.198	0.920	1.118
BM LSC1000	-0.187	0.893	1.080

In order to quantitatively evaluate the catalytic activity of the perovskite catalysts for ORR, mass activity and specific activity were calculated from the ORR curves and are shown in Fig. 6. Mass and specific activities were calculated at -0.20, -0.25 and -0.30 V vs. Hg/HgO, respectively. The synthesized LSC1000 catalyst shows higher catalytic activity than LSC900 and KB. It can be clearly seen from Figure 6 that the catalytic activity of the LSC catalysts are greatly enhanced after ball milling which is attributed to the increase in specific surface area and/or the formation of reactive defects in the structures. Especially, BM LSC1000 shows the highest mass activity and specific activity among all other perovskite catalysts. The highest catalytic activity of the BM LSC1000 is due to the absence of impurity.

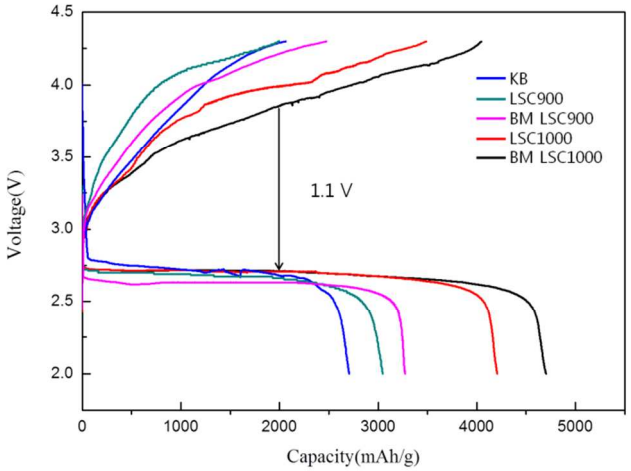

Fig.7 The first charge- discharge profiles of LSC catalyzed Li-O2 battery in comparison without catalyst

Cite this: DOI: 10.1039/c0xx00000x

www.rsc.org/xxxxxx

ARTICLE TYPE

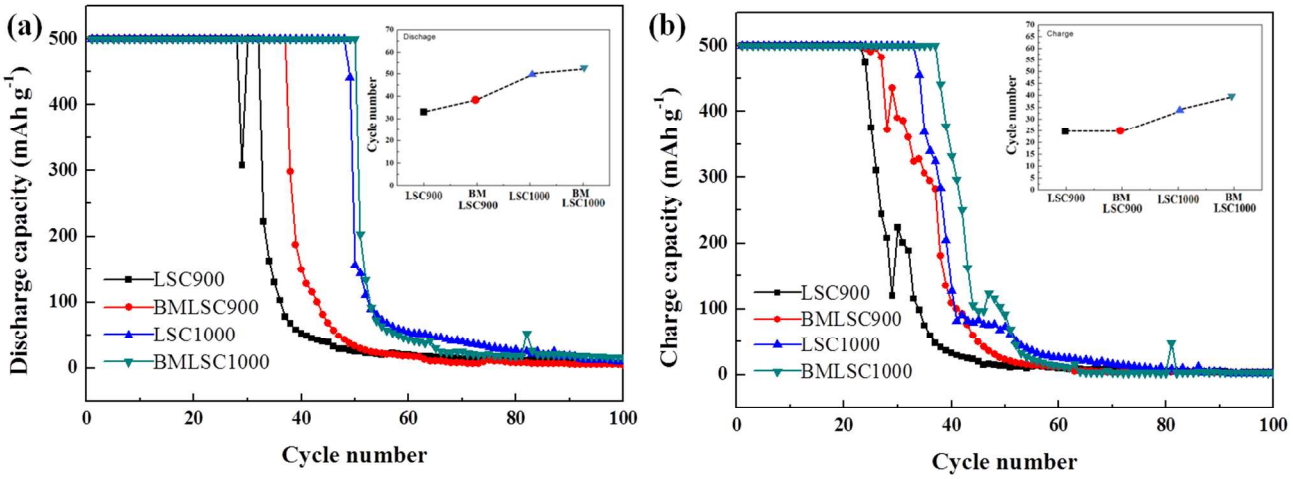

Fig. 8 Cycle life efficiency of the lithium-air battery using the $La_{0.6}Sr_{0.4}CoO_{3-\delta}$ perovskite catalysts (a) discharge and (b) charge

3.3 Lithium air battery performance of perovskite $La_{0.6}Sr_{0.4}CoO_{3-\delta}$

With the ORR and OER activities of the perovskite oxide catalysts proven in the LSV experiments and other electrochemical characterization, the catalysts were applied to Li air battery. The lithium–air battery was constructed using the synthesized perovskite catalysts and the charge–discharge performance of the battery was evaluated with 1M LiTFSI (TEGDME) in Swagelok™ type cells. The cells were tested at a constant current density of 0.1mA/cm^2 in a potential range of 2.0–4.3V at room temperature and O_2 atmosphere. The KB air cathode with and without catalyst were tested versus (Li/Li$^+$) lithium metal anode and their first charge–discharge profiles are given in Fig. 7. From this figure, it can be clearly seen that the addition of catalysts has increased the capacity of the cells. The first discharge curve of LSC 1000 reached a maximum capacity of ~4208mAh/g with a flat discharge plateau at 2.75V. The obtained capacity is higher than that of the Li-O_2 cells with LSC 900 (~3047mAh/g) and without any catalyst (~2706mAh/g). In addition, the ball milled samples (BM LSC 900 and 1000) considerably improves the capacity, and BM LSC 1000 showed a maximum first capacity of 4701mAh/g. On charging a maximum of 86% capacity retention is achieved with the capacity of 4000mAh/g. Also, the difference in discharge and charge potential or overpotential, ΔV is 1.1V which is very low and favourable for the reversibility of the battery. It is clearly seen that the addition of BM LSC 1000 has increased the specific capacity and reduced the over potential of the Li air battery than that of other cells with and without any catalysts. This attests to the fact that addition of perovskite LSC catalyst has efficiently increased the performance of the cell.

To obtain complete stable cycling without any fade in the capacity we investigated the cells with a limited depth of discharge. Considerable cycling performance can be improved by limiting the depth of discharge and charging [51]. The cycle life and efficiency of the battery were measured with a limited capacity of 500mAh g^{-1} at 0.1mA cm^{-2}, as given in Fig.8. It can be seen that discharge and charge capacity of LSC1000 are considerably better than those of LSC900. In addition, the ball milled samples (BM LSC 900 and 1000) considerably improves the cyclability of the battery during cycling, as observed in Fig.8. Particularly, the discharge and charge capacities of BM LSC1000 were considerably improved during cycling than other perovskite oxides. BM LSC1000 cycling data shows a uniform discharge/charge up to 38 cycles without any capacity fade. However, after 38 cycles, the charge capacity was gradually decreased (shown in Fig. 8(b)). This capacity fade can be attributed to slow oxidation kinetics of Li_2O_2 formed upon discharge. These observations are consistent with the previous studies on lithium air batteries [52–54]. On the other hand, BM LSC900 was stable only up to 24 cycles, and the charge capacity was gradually reduced after that. One important observation from the charge/discharge behaviour is the enhanced battery performance of all the ball milled samples which is due to increased specific surface area and/or the formation of reactive defects in structures upon ball milling. High specific surface area eventually provides more active sites for the electrochemical reaction. These results further confirm the electrochemical observations in which the BM LSC1000 showed much better performance in comparison with BM LSC900, which is attributed to the pure phase structure of BM LSC1000. Furthermore, the improved cycling performance may be due to the unique properties of the electrode structure of BM LSC1000 catalyst, which facilitate the formation and decomposition of the discharge product and thus improve the reversibility of the O_2 electrode.

4. Conclusions

Perovskite $La_{0.6}Sr_{0.4}CoO_{3-\delta}$ was synthesized using the Pechini method with different drying and calcination temperatures for the application as air cathode catalyst in lithium–air batteries. XRD spectra showed that regardless of the drying temperatures the synthesized LSC oxides at 1000°C exhibited the stable perovskite structure without the formation of any impurities. From FESEM and TEM analyses, it could be observed that the primary particles aggregate to form secondary particles resulting in the larger sizes of the perovskite LSC oxides. From the electrochemical characterizations, the perovskite LSC exhibited better catalytic performance than conventionally used KB. The catalytic activity of LSC1000 was found to be better than that of LSC900. The ball milled LSC showed better catalytic performance due to their improved surface properties. These promising results suggest that the synthesized perovskite LSC can be used as air cathode for the next generation lithium-air batteries.

Acknowledgement

This work was supported by the Human Resources Development program (NO. 20134030200330) of the Korea Institute of Energy Technology Evaluation and Planning (KETEP) grant funded by the Korea government Ministry of Trade, Industry and Energy.

Notes and references

[a]R&D Education Center for Fuel Cell Materials & Systems, [b]Department of Energy Storage and Conversion Engineering, [c]School of Chemical Engineering, Chonbuk National University, Jeonju 561-756, Republic of Korea.

**Corresponding author: Fax: +82 63 270 3909; Tel: +82 63 270 2311; E-mail: nahmks@jbnu.ac.kr (K.S.Nahm)*

1 E. Hosono, T. Kudo, I. Honma, H. Matsuda and H. Zhou, *Nano Lett*., 2009, **9(3)** 1045–1051.
2 J. Xiao, D. Wang, W. Xu, D. Wang, R.E. Williford, J. Liu and J. Zhang, *J. Electrochem. Soc*., 2010, **157**, A487–A492.
3 E.K. Kim, B.H. Choi, M.J. Ji, S.H. Jung and K.B. Kim, *Korean J. Met. Mater.*, 2013, **51(3)**, 227–232.
4 H.R. Bak, J.H. Lee, B.K. Kim and, W.Y. Yoon, *Electron. Mater. Lett.*, 2013, **9(2)**, 195–199.
5 J. Tarascon and M. Armand, *Nature*, 2001, **414**, 359–367.
6 A.R. West, *Basic Solid State Chemistry*. 2nd ed., 1999.
7 J.M.D. Coey, M. Viret and S. von Molnar, *Advances in Physics*, 1999, **48(2)**, 167–293.
8 G. Girishkumar, B. McCloskey, A. Luntz, S. Swanson and W. Wilcke, *J. Phys. Chem. Lett.,* 2010, **1**, 2193–2203.
9 C. Park, S. Park, S. Lee, H. Lee, H. Jang and W. Cho, *Bull. Kor. Chem. Soc.,* 2010, **31**, 3221–3224.
10 H. Jung, J. Hassoun, J. Park, Y. Sun and B. Scrosati, *Nature* Chem., 2012, **4**, 579–585.
11 B. McCloskey, A. Speidel, R. Scheffler, D. Miller, V. Viswanathan, J. Hummelshøj, J. Nørskov and A. Luntz, *J. Phys. Chem. Lett.,* 2012, **3**, 997–1001.
12 Y. Shao, S. Park, J. Xiao, J. Zhang, Y. Wang and J. Liu, *ACS Catalysis*, 2012, **2**, 44–857.
13 B. Kumar, J. Kumar, R. Leese, J. P. Fellner, S. J. Rodrigues and K. M. Abraham, *J. Electrochem. Soc*., 2010, **157**, A50–A54.
14 J. Read, K. Mutolo, M. Ervin, W. Behl, J. Wolfenstin, A. Driedger and D. Foster, *J. Electrochem. Soc*., 2003, **150**, A1351–A1356.
15 A. Debart, J. Bao, G. Armstrong and P. G. Bruce, *J. Power Sources*, 2007, **174**, 1177–1182.
16 Y.C. Lu, Z. Xu, H. A. Gasteiger, S. Chen, K. H. Schifferli and Y. S. Horn*, J. Am. Chem. Soc*., 2010, **132**, 12170–12171.
17 A. Debart, A. J. Paterson, J. Bao and P. G. Bruce, *Angew Chem.,Int. Ed.,* 2008, **47**, 4521–4524.
18 H. Cheng and K. Scott, *J. Power Sources*, 2010, **195**, 1370–1374.
19 V.M.B. Crisostomo, J. K. Nagala, S. Alia, A. Dobley, C. Morein, C. H. Chen, X. Shen, S. L. Suib, *Chem. Mater.,* 2007, **19**, 1832–1839.
20 Y.C. Lu, H.A. Gasteiger, M.C. Parent, V. Chiloyan, Y. Shao-Horn, Electrochem. Solid State Lett. 13(6) (2010) A69–A72.
21 A. Zahoor, M. Christy, Y.J. Hwang and K.S. Nahm*, Journal of Electrochem. Sci. and Technol*., 2012, **3(1)**, 14–23.
22 G. Gnanakumar, A. Zahoor and K.S. Nahm, *J.S. Xavier Biosens. and Bioelectron*., 2014, **53**, 528–534.
23 Bing Sun, Hao Liu, Paul Munroe, Hyojun Ahn, and Guoxiu, *Nano Res*., 2012, **5(7)**, 460–469.
24 X. Han, Y. Hu, J. Yang and F. Cheng, *J. Chen, Chem. Commun*., 2014, **50**, 1497–1499.
25 Z. Fu, X, Lin, T. Huang and A, Yu, *J. Solid State Electrochem.,* 2012, **16**, 1447–1452.
26 Ji-Jing Xu, Dan Xu, Zhong-Li Wang, Heng-Guo Wang, Lei-Lei Zhang, and Xin-Bo Zhang, *Angew. Chem. Int. Ed*., 2013, **52**, 3887–3890.
27 Yunlong Zhao, Lin Xu, Liqiang Mai, Chunhua Han, Qinyou An, Xu Xu, Xue Liu, and Qingjie Zhang*,, PNAS Early Edition*, 2012.
28 K.N. Jung, J.H. Jung, W.B. Im, S. Yoon, K.H. Shin and J.W. Lee, *Appl. Mater. Interfaces*, 2013, **5**, 9902**–**9907.
29 H. Ohkuma, I. Uechi, N. Imanishi, A. Hirano, Y. Takeda and O. Yamamoto, *Journal of Power Sources*, 2013, **223**, 319–324.
30 Chao Jin, Zhibin Yang, Xuecheng Cao, Fanliang Lu and Ruizhi Yang, *International journal of hydrogen energy*, 2013, **39**, 2526-2530.
31 Ji-Jing Xu, Zhong-Li Wang, Dan Xu, Fan-Zhi Meng and Xin-Bo Zhang, *Energy Environ. Sci*., 2014, **7**, 2213-2219
32 Zhenzhen Du, Peng Yang, Long Wang, Yuhao Lu, J.B. Goodenough and Jian Zhang,Dawei Zhang, *J Power Sources*, 2014, **265**, 91-96.
33 Andreas Egger, Edith Bucher, Min Yang and Werner Sitte, *Solid State Ionics*, 2012, **225**, 55–60.
34 Cahit Benel, Azad J. Darbandi, Ruzica Djenadic, Anna Evans, René Tölke, Michel Prestat and Horst Hahn, *Journal of Power Sources*, 2013, **229**, 258-264.
35 Per Hjalmarsson, Martin Søgaard and Mogens Mogensen, *Solid State Ionics*, 2008, **179**, 1422–1426.
36 Edith Bucher, Werner Sitte, Frederik Klauser and Erminald Bertel, *Solid State Ionics*, 2012, **208**, 43–51.
37 S. Trasatti, *Elsevier Scientific Publishing Co*, 1981, 521–626.
38 L.W. Tai, M. M. Nasrallah, H. U. Anderson, D. M. Sparlin and S. R. Sehlin, *Solid State Ionics*, 1995, **76**, 273–283.
39 T. Nakamura, M. Misono and Y. Yoneda, *Bull. Chem. Soc. Jpn.*, 1982, **55(2)**, 394–399.
40 M. P. Pechini. *American Patent*, 1967, 3 330 697,.
41 K.D. Budd, D.A. Payne, Better Ceramics through chemistry, eds. C.J. Brinker, D.E. Clark and D.R. Ulrich, *New York*, 1984, 239–244.
42 T. Nitamori, S. Kurihara and M. Misono, *J. Catal*., 1986, **98(1)**, 221–228.
43 V. Esposito, M. Søgaard and P.V. Hendriksen, *Solid State Ionics*, 2012, **227**, 46–56.
44 M.J. Scholten, J. Schoonman, J.C. van Miltenburg and H.A.J. Oonk, *Solid State Ionics*, 1993, **61**, 83–91.
45 B.H. Erné, A.J. van der Weijden, A.M. van der Eerden, J.B.H. Jansen, J.C. van Miltenburg and H.A.J. Oonk, *Calpha*d, 1992, **16**, 63–72.
46 P. Scherrer and N.G.W. Gottingen, *Math-Phys. Kl*., 1918. **2**, 96–100.
47 J.I. Langford and A.J.C. Wilson, *Journal of Applied Crystallography*, 1978, **11**, 102–113.
48 W. Zhou, Z. Shao, R. Ran, H. Gu, W. Jin and N. Xu, *J. Am. Ceram. Soc*., 2008, **91(4)**, 1155–1162.
49 Y. Gorlin and T.F. Jaramillo, *J. Am. Chem. Soc*., 2010, **132**, 13612–136124.
50 Y. Matsumoto and E. Sato, *Mater. Chem. Phys*., 1986, **14**, 397–426.
51 Y.M. Cui, Z.Y. Wen, X. Liang, Y. Lu, J. Jin, M.F. Wu and W. Wu, *Energy Environ. Sci*., 2012, **5**, 7893–7897.
52 S. Ida, A.K. Thapa, Y. Hidaka, Y. Okamoto, M. Matsuka, H. Hagiwara and T. Ishihara, *J. Power sources*, 2012, **203**, 159–164.

53 G.Q. Zhang, J.P. Zheng, R. Liang, C. Zhang, B. Wang, M. Au, M. Hendrickson and E.J. Plichta, *J. Electrochem. Soc*., 2011, **158**, A822–A827.

54 T. Ogasawara, A. Debart, M. Holzapfel, P. Novak and P.G. Bruce, *J. Am. Chem. Soc*., 2006, **128**, 1390–1393.